PSFC/JA-00-33

Observations of Toroidal Rotation Suppresion with ITB Formation in ICRF and Ohmic H-mode Alcator C-mod Plasmas

J.E. Rice, R.L. Boivin, P.T. Bonoli, J.A. Goetz, R.S. Granetz
M.J. Greenwald, I.H. Hutchinson, E.S. Marmar, J.A. Snipes, S.M. Wolfe,
S.J. Wukitch, C.L. Fiore, J.H. Irby, D. Mossessian, M. Porkolab

October 2000

Plasma Science and Fusion Center
Massachusetts Institute of Technology
Cambridge, MA 02139 USA

This work was supported by the U.S. Department of Energy, Cooperative Grant No. DE-FC02-99ER54512. Reproduction, translation, publication, use and disposal, in whole or in part, by or for the United States government is permitted.

Submitted for publication to *Nuclear Fusion.*

Observations of Toroidal Rotation Suppression with ITB Formation in ICRF and Ohmic H-mode Alcator C-Mod Plasmas

J. E. Rice, R. L. Boivin, P. T. Bonoli, J. A. Goetz, R. S. Granetz,
M. J. Greenwald, I. H. Hutchinson, E. S. Marmar, J. A. Snipes, S. M. Wolfe,
S. J. Wukitch, C. L. Fiore, J. H. Irby, D. Mossessian and M. Porkolab
Plasma Science and Fusion Center, MIT, Cambridge, MA 02139-4307

Abstract

Co-current central toroidal rotation has been observed in Alcator C-Mod plasmas with on-axis ICRF heating. The rotation velocity increases with plasma stored energy and decreases with plasma current. Very similar behavior has been seen during Ohmic H-modes, which suggests that the rotation, generated in the absence of an external momentum source, is not principally an ICRF effect. A scan of the ICRF resonance location across the plasma has been performed in order to investigate possible influences on the toroidal rotation. With a slight reduction of the toroidal magnetic field from 4.7 to 4.5 T and a corresponding shift of the ICRF resonance from r/a = −0.36 to −0.48, the central toroidal rotation significantly decreased in concert with the formation of an internal transport barrier (ITB). During the ITB period, the electrons and impurities peaked continuously for $|r/a| \leq 0.5$. Comparison of the observed rotation and neo-classical predictions indicates that the core radial electric field changes from positive to negative during the ITB phase. Similar rotation suppression and ITB formation have been observed during some Ohmic H-mode discharges.

I. Introduction

There is a strong connection between plasma rotation, the transition from L- to H-mode and the formation of transport barriers in tokamak plasmas [1,2]. Furthermore, in advanced tokamak operational scenarios [3,4,5], an internal transport barrier (ITB) is desired to provide additional confinement enhancement and to drive bootstrap current. Improved energy confinement and steep rotation velocity profiles are intimately tied together, and are linked to ITB formation [6,4,5]. When the E×B shearing rate, which is proportional to the rotation velocity gradient, exceeds the maximum growth rate for ion temperature gradient driven (ITG) microturbulence, the ion thermal conductivity reduces to neo-classical levels, and an improvement of energy confinement ensues. Discharges with ITBs exhibit this behavior over the entire plasma cross section [4]. Most observations of rotation [7-9] and ITB formation [3-5] have been made in plasmas with an external momentum and particle source, usually provided by neutral beams. Interpreting the rotation measurements with regard to the association with H-mode is complicated by the contribution to the rotation from the direct momentum input of the neutral beams. Similarly, it is difficult to separate the influence of changes in particle transport to internal particle transport barrier formation from the contributions of particles originating directly from the neutral beams. Heating only by ICRF waves and purely Ohmic H-modes provide the opportunity for the study of toroidal rotation and ITB formation in plasmas with no direct momentum or particle input. Co-current rotation in ICRF plasmas [10-13] and Ohmic H-mode discharges [14,15] has been documented. The mechanism which drives this rotation in the absence of direct momentum input remains unknown.

Within the framework of the standard neo-classical treatment of rotation [16,17], expanded to include impurity species properly [18], the toroidal rotation is given as a function of the ion density and temperature gradients and the radial electric field, E_r. However, E_r is not calculated from first principles, and is not easily measured directly. E_r is routinely inferred from measured impurity rotation and the

force balance equation [19]. Alternately, there have been several calculations taking the approach that the toroidal rotation observed in ICRF heated discharges is an ICRF effect. The direct momentum absorption of ICRF waves by ions has been calculated for JET plasmas [10], and is found to be small, in the counter-current direction and therefore not an important factor in producing the observed rotation. Non-ambipolar radial transport, through shifts of resonant ion orbits [20,21], has been considered in generating E_r and plasma rotation. Toroidal rotation driven by toroidally directed ICRF waves has been calculated [22] and toroidal rotation associated with a special class of magnetosonic-whistler modes excited by ICRF waves has also been considered [23].

In this paper, recent results of impurity toroidal rotation measurements in ICRF and Ohmic H-mode Alcator C-Mod plasmas are presented. In Section II the experimental setup is described, and the correlation between the velocity increase and the plasma stored energy increase (confinement improvement) is demonstrated. The inverse relationship between the rotation velocity and the plasma current is noted for both ICRF and Ohmic H-mode discharges. Observations of the suppression of the co-current toroidal rotation together with the formation of internal transport barriers are presented in Section III. Comparisons of observed rotation velocity profiles with those calculated from neo-classical theory are made in Section IV, and similarities with ITB formation in Ohmic plasmas are presented. Conclusions are drawn in Section V.

II. Toroidal Rotation during ICRF and Ohmic H-modes

The observations presented here were obtained from the Alcator C-Mod [24] tokamak, a compact (major radius R = 0.67 m, typical minor radius of 21 cm, and elongation $\kappa \leq 1.8$), high field device ($2.6 \leq B_T \leq 8.0$ T) in the lower single null configuration, which has operated with plasma currents between 0.23 and 1.5 MA and volume averaged electron densities between 0.24 and 5.9 $\times 10^{20}/m^3$. Up to 4

MW of ICRF power at 80 MHz [25] are available, and the power is coupled to the plasma by 2 two-strap antennas, each with $0 - \pi$ phasing; the cases described here are with H minority heating in deuterium plasmas. On-axis heating occurs for a toroidal magnetic field of 5.3 T. Central electron and ion temperatures are in the range from 1 to 5 keV. For central toroidal rotation measurements, x-ray spectra were recorded with a spatially fixed von Hamos type crystal x-ray spectrometer [26], whose line of sight is tangent to the plasma axis, pointing in the counter current direction during normal current operation. Central rotation velocities have been determined from the Doppler shifts of the Ar^{17+} Ly_α doublet [27]. Off-axis rotation velocities were determined from the forbidden line z in Ar^{16+}, observed with a five chord, spatially (vertically) scannable x-ray spectrometer array [28], with a slight toroidal view. Spectra are typically collected every 20 ms during plasma discharges, and averaged over the sawtooth oscillations which are normally present. Argon is routinely injected into Alcator C-Mod plasmas through a piezoelectric valve, to provide x-ray transitions for Doppler width ion temperature measurements [29]. Statistical errors in the deduced rotation velocities from fits to the line positions depend on the counting rate and are usually less than 5×10^3 m/s. Systematic errors in the absolute rotation velocities can be as large as 1×10^4 m/s, but are eliminated in all scalings which show the change in the rotation velocity before and during both ICRF injection periods and Ohmic H-mode phases. Rotation velocities were independently determined from sawtooth pre- and post-cursors as measured from magnetic pick-up coils [14], with good agreement between the two diagnostics.

Electron density profiles were determined from the visible continuum using a high spatial resolution imaging CCD system [30]. Comparison of these *bremsstrahlung* profiles with the electron density profiles measured by Thomson scattering, which has only six spatial locations in the core plasma, allows Z_{eff} as a function of radius to be determined. The Z_{eff} profiles were interpolated, and used to convert the *bremsstrahlung* profiles into full electron density profiles with fine spatial resolution. This correction is proportional to $\sqrt{Z_{eff}}$ and is typically less than 20%. In some discharges with impurity peaking, the correction can be as large as 70%. Soft x-ray

brightness profiles were measured with two 38 channel diode arrays [31]. Spatial and temporal resolution for this diagnostic, which is sensitive to x-rays with hν > 2 keV, are 2.5 cm and 30 μsec, respectively.

Shown in Fig.1 is a comparison of the central toroidal rotation velocity in two similar discharges that had normal and reversed plasma current (top frame). Both plasmas had on-axis heating with comparable ICRF power levels (third panel) and subsequent stored energy increases (second frame); the changes in the rotation velocities (bottom panel) were of similar magnitude but in opposite directions, remaining co-current. The time histories of the rotation velocities were very similar to the plasma stored energy time histories [11,12], although for the reversed current case the rotation velocity was 'negative'. There was a delay, about equal to the energy confinement time, of the modulations in the velocity traces relative to the stored energy signals [11,12]. The relationship between the rotation velocity, stored energy and plasma current is summarized in Fig.2; this is a comparison between the rotation velocity increase before and during ICRF and Ohmic H-modes and the plasma stored energy increase normalized to the plasma current, before and during ICRF and Ohmic H-modes. All of the ICRF data are for plasmas with the resonance close to the magnetic axis. The ICRF H-mode points are sorted by plasma current; there is a larger velocity increase for a given stored energy increase at lower plasma current [12]. The Ohmic H-mode points display a similar trend, although the stored energy increases are modest since with only Ohmic power input, it is difficult to exceed the H-mode threshold. The Ohmic points have not been sorted by plasma current, but the range presented in the figure is from 0.8 to 1.4 MA, which also explains why the rotation velocity increases are modest compared to the ICRF points. This common trend suggests that the co-current toroidal rotation is probably not driven by the ICRF waves or energetic particle effects [14].

III. Toroidal Rotation Suppression with ITB Formation

In an effort to study the effects of off-axis ICRF heating on the toroidal rotation velocity, and to investigate the predicted reversal of the rotation velocity with the ICRF resonance located inside of the magnetic axis [21], Alcator C-Mod was operated with toroidal magnetic fields other than the nominal value of 5.3 T (which corresponds to on-axis absorption). Shown in Fig.3 is a comparison of parameters for two consecutive discharges, with magnetic fields of 4.7 and 4.5 T. Both discharges had similar target plasma parameters (0.8 MA of plasma current, central electron density of $1.8 \times 10^{20}/\mathrm{m}^3$ and a hydrogen-to-deuterium ratio of 0.03), and 2.7 MW of ICRF power. In the 4.7 T case, with the ICRF resonance location at -7.5 cm in minor radius, the normal co-current toroidal rotation (bottom frame) was observed throughout the ICRF pulse. When the magnetic field was lowered further to 4.5 T, with the resonance at -10 cm, the plasma initially began rotating in the co-current direction, but after 0.9 s into the discharge, an internal transport barrier formed (at $\sim$10 cm) and the toroidal rotation velocity slowed down and reversed direction. In this ITB discharge there was a continuous peaking of the electron density profile (third panel), between 0.9 and 1.2 s. The plasma stored energy (top frame) and central ion temperature (second panel) in these two discharges were similar up until 1.2 s. The results of the complete toroidal magnetic field/resonance location position scan are shown in Fig.4. This set of discharges had similar ICRF power levels (and waveforms) and target plasma densities, while the toroidal magnetic field was scanned shot to shot at a plasma current of 0.8 MA. In the top frame are shown the toroidal rotation velocity and the increase in the plasma stored energy (compared to the pre-RF values), for the time interval between 0.75-0.95 s. This scan covers $\mathrm{B_T}$ between 4.1 and 6.05 T, with the resonance location varying between -15.2 and $+9.9$ cm. There are only very subtle changes of the rotation velocity and stored energy, with a slight reduction of these quantities perhaps at the extreme ends of the scan. Certainly there is no reversal of the rotation direction with the ICRF resonance location on the inboard (negative) side during this time interval. These results are confirmed by observations of the rotation from an analysis of sawtooth pre- and post-cursors from the magnetics measurements, and this is similar to what

was seen in a previous scan of the toroidal field (Fig.8, Ref.[12]) where a substantial drop in the rotation and stored energy was observed only with the resonance located outside of +15 cm. The situation is different during the time interval from 1.0-1.2 s, as shown in the bottom frame of Fig.4. While the plasma stored energy exhibits the same trend as in the top frame, there is a significant change in the toroidal rotation velocity at this later time with the resonance location outside of −8 cm, and $B_T \leq 4.6$ T. Unfortunately there are few data points for this late time during the discharge with the resonance location greater than +5 cm because the ICRF power repeatedly tripped. (However, from Fig.8 of Ref.[12], there was no sudden decrease in the rotation velocity when the field was raised up to 6.6 T.) For a slight 0.1 T reduction in B_T below 4.7 T (or a 1 cm shift in the resonance location outside of −8 cm) there is an abrupt decrease in the central rotation velocity 200 ms after the initiation of the ICRF pulse. The discharges with the resonance location outside of −8 cm that undergo a reduction of the rotation velocity after 1.0 s also exhibit formation of a particle ITB.

Two manifestations of the ITB are demonstrated in Fig.5 where the time evolution of the electron density and soft x-ray brightness profiles are shown for the 4.5 T discharge of Fig.3. There is a continuous peaking of both of these profiles throughout the duration of the ICRF pulse inside of R = 0.785 m (r = 10 cm), with little variation outside of this radius. The magnetic axis for this discharge was located near R = 0.693 m. There is an H-mode edge density pedestal which persists throughout the ICRF injection, including during the ITB formation. The location of the foot of the ITB is inside of 10 cm in minor radius, very close to the resonance location for this discharge. However, this may just be a coincidence since for discharges with an ITB produced by pellet injection (without ICRF), the location of the break in the electron density profile is also near 10 cm. (see below). Interestingly, this 4.5 T, ITB discharge underwent sawtooth oscillations up until 1.20 s, and the location of the sawtooth inversion radius was ∼0.722 m in major radius, or ∼2.5 cm in minor radius, well inside the ITB boundary radius and the ICRF resonance. It's remarkable that this strong density peaking persisted in the

presence of sawtooth oscillations. After the termination of the sawtooth oscillations, a nipple quickly formed at the peak of the electron density profile inside of r = 2.5 cm.

Some radial profile information on the toroidal rotation velocity is available from the scanning x-ray spectrometer array. Shown in Fig.6 are the rotation time histories for the 4.5 T discharge of Fig.3 from three different lines of sight: the central chord, fully tangential sight line, and two views with equal toroidal angles ($\sim 10^\circ$ counter clockwise) and opposite poloidal lines of sight, which intersect the vertical midplane at ± 10.4 cm. These off-axis views map to the midplane at R = 0.770 m or r = 7.5 cm, accounting for the plasma elongation. Since all three of these time histories are similar, it can be concluded that any poloidal contribution to the rotation at a minor radius of 7.5 cm is small, and that the toroidal rotation velocity profile out to this radius is relatively flat [14].

IV. Comparison with Neo-Classical Theory and Discussion

The observed toroidal rotation velocities before and during the ITB formation may be compared with the predictions of neo-classical theory. The impurity toroidal rotation velocity has been determined by solving the parallel momentum and heat flow balance equations [18],

$$V_T^I = \frac{1}{B_P}\left[E_r + \frac{(K_1 + \frac{3}{2}K_2 - 1)}{e}\frac{\partial T_i}{\partial r} - \frac{T_i}{e n_i}\frac{\partial n_i}{\partial r}\right] \qquad (1).$$

Here the subscripts T and P denote toroidal and poloidal, T_i and n_i are the ion temperature and density, K_1 and K_2 are of order unity and are functions of the viscosity matrix elements, inverse aspect ratio and the impurity strength parameter (evaluated for all collisionality regimes in the appendix of Ref.[18]) and E_r is the radial electric field. Equation 1 has been evaluated for the discharge of Figs.5 and 6 before and during the ITB. The poloidal magnetic field was calculated from the magnetics reconstruction code EFIT [32], and the measured electron density and

temperature profiles were used for the ion profiles. The only quantity not measured directly was the radial electric field, which can be determined from a comparison with the observed rotation velocity profile. The calculated toroidal rotation velocity profile, without the E_r/B_P term in Eq.(1), for the pre-ITB H-mode phase of the 4.5 T discharge of Figs.3, 5 and 6 is shown in the top frame of Fig.7. The computed profile is flat, and near zero, across most of the plasma, with a sharp increase in the neighborhood of the edge pedestal [12]. The measured points are also shown. In order to make the calculated velocity profile agree with the observations, a radial electric field of 12 kV/m at r = 7.5 cm [11] is required. The situation is very different during the ITB portion of the discharge, as seen in the bottom frame of Fig.7. While the edge pedestal remains the same, there is a large (co-current) bump ($\sim 3 \times 10^4$ m/s) predicted in the toroidal rotation velocity profile at the location of the ITB, where the density gradient is large. Here the observed rotation velocity is near zero or slightly negative (counter-current), which implies that E_r has reversed sign, with a value of -18 kV/m. This reversal of E_r has been noted during ITB formation in D III-D [4].

As mentioned above, it is probably fortuitous that the foot of the ITB is very close to the ICRF resonance location (Fig.5). Suppression of the co-current toroidal rotation in conjunction with ITB formation has also been observed in some Ohmic H-mode plasmas. Shown in Fig.8 are parameter time histories for an Ohmic H-mode discharge which developed an ITB. During the normal Ohmic H-mode phase ($t < 1.10$ s), the plasma was rotating in the co-current direction [14,15] at 50 km/s. At 1.13 s, an internal transport barrier began to form, with strong increases in electron density peaking, the central soft x-ray emission and the central ion temperature. Simultaneous with these increases was an equally strong reduction in the central rotation velocity, very similar to what was seen in Fig.3. In this case the ITB formation and velocity suppression are clearly not due to ICRF effects. Further evidence that it is just a coincidence that the ITB boundary position and the ICRF resonance location are close may be revealed by an examination of the electron density profiles in both Ohmic and off-axis ICRF heated ITB discharges.

Shown in Fig.9 are electron density profiles measured during the ITB phase of three separate discharges: an Ohmic H-mode ITB plasma, and two ICRF discharges with the resonance location at -9.9 and -12.4 cm. In all three cases the ITB location was inside of r = $\sim$10 cm; there was no shift in the ITB foot position when the resonance location was moved. With the ICRF resonance at -7.5 cm, there was no ITB formation at all (Fig.4). It is not understood why the ITB forms inside of r = 10 cm in all three cases but this is very close to the location of the maximum of the poloidal magnetic field.

V. Conclusions

Co-current central toroidal rotation has been observed in ICRF and Ohmic H-mode plasmas. Similar scalings of the rotation velocity with plasma stored energy and current in both types of discharge imply that the rotation is not principally an ICRF effect. The mechanism which drives this rotation in the absence of external momentum input remains unknown. With off-axis ICRF heating, some plasmas exhibit the formation of internal particle transport barriers and a slowing down of the toroidal rotation. Some Ohmic H-mode discharges also undergo ITB formation and rotation suppression. A comparison of the observed rotation with the predictions of neo-classical theory implies a negative core radial electric field during the ITB phase. How the ITB forms with off-axis ICRF heating and why the ITB forms inside of r/a = 0.5 are unexplained.

VI. Acknowledgements

The authors thank F. Perkins and R. White for useful discussions, J. Terry for D_α measurements, A. Hubbard for electron temperature measurements, G. Schilling for assistance with the ICRF system and the Alcator C-Mod operations and RF groups for expert running of the tokamak. Work supported at MIT by DoE Contract No. DE-FC02-99ER54512.

References

[1] K. C. Shiang and E. C. Crume, Phys. Rev. Lett. **63** (1989) 2369.

[2] K. H. Burrell et al., in *Plasma Physics and Controlled Nuclear Fusion Research 1994* Proceedings of the 15th International Conference, Seville, Spain, Vol.1 (IAEA, Vienna 1996) 221.

[3] T. Oikawa et al., Nucl. Fusion **40** (2000) 1125.

[4] V. S. Chan et al., Nucl. Fusion **40** (2000) 1137.

[5] O. Gruber et al., Nucl. Fusion **40** (2000) 1145.

[6] G. M. Staebler et al., Nucl. Fusion **37** (1997) 287.

[7] K. H. Burrell et al., Nucl. Fusion **28** (1988) 3.

[8] N. Asakura et al., Nucl. Fusion **33** (1993) 1165.

[9] Y. Miura et al., Plasma Phys. Contr. Fusion **40** (1998) 799.

[10] L.-G. Eriksson et al., Plasma Phys. Contr. Fusion **39** (1997) 27.

[11] J. E. Rice et al., Nucl. Fusion **38** (1998) 75.

[12] J. E. Rice et al., Nucl. Fusion **39** (1999) 1175.

[13] G. T. Hoang et al., Nucl. Fusion **40** (1999) 913.

[14] I. H. Hutchinson et al., Phys. Rev. Lett. **84** (2000) 3330.

[15] J. E. Rice et al., Phys. Plasmas **7** (2000) 1825.

[16] F. L. Hinton and R. D. Hazeltine, Rev. Mod. Phys. **48** (1976) 239.

[17] S. P. Hirshman and D. J. Sigmar, Nucl. Fusion **21** (1981) 1079.

[18] Y. B. Kim, P. H. Diamond and R. J. Groebner, Phys. Fluids B **3** (1991) 2050.

[19] K. Ida, Plasma Phys. Contr. Fusion **40** (1998) 1429.

[20] C. S. Chang et al., Phys. Plasmas **6** (1999) 1969.

[21] F. W. Perkins et al., Proceedings of the 27th European Physical Society Conference on Controlled Fusion and Plasma Physics, Budapest, 2000 paper OR01.

[22] T. Hellsten et al., in *Plasma Physics and Controlled Nuclear Fusion Research 1998* Proceedings of the 17th International Conference, Yokohama, IAEA-F1-CN-69/THP2/36.

[23] B. Coppi et al., in *Plasma Physics and Controlled Nuclear Fusion Research*

1998 Proceedings of the 17th International Conference, Yokohama, IAEA-F1-CN-69/TH3/7.

[24] I. H. Hutchinson et al., Phys. Plasmas **1** (1994) 1511.

[25] S. N. Golovato, M. Porkolab, Y. Takase et al., in *Proceedings of the 11th Topical Conference on Radio-Frequency Power in Plasmas*, Palm Springs, CA 1995, AIP Conference Proceedings 355 (Editors: Ronald Prater, Vincent S. Chan) American Institute of Physics, Woodbury, New York 1996 p.23

[26] E. Källne, J. Källne, E. S. Marmar and J. E. Rice, Phys. Scr. **31** (1985) 551.

[27] E. S. Marmar et al., Phys. Rev. A **33** (1986) 774.

[28] J. E. Rice and E. S. Marmar, Rev. Sci. Instrum. **61** (1990) 2753.

[29] J. E. Rice et al., Rev. Sci. Instrum. **66** (1995) 752.

[30] E. S. Marmar et al., accepted for publication Rev. Sci. Instrum. (2000).

[31] R. S. Granetz and L. Wang, in *International School of Plasma Physics-9, 1991, Proceedings of Diagnostics fo Contemporary Fusion Experiments, Varenna, Italy* Editrice Compositori, Bologna, Italy, p.425.

[32] L. L. Lao et al., Nucl. Fusion **25** (1985) 1611.

Figure Captions

Fig. 1 A comparison of rotation during ICRF heated plasmas with forward (red dash-dot-dot-dot lines) and reversed (solid green lines) plasma current.

Fig. 2 The change in the toroidal rotation velocity (the difference between the H-mode and pre-H-mode values) as a function of the change in the plasma stored energy normalized to the plasma current, for Ohmic and ICRF (with on axis heating) H-modes. The Ohmic values are all shown as purple dots, unseparated in plasma current, while the ICRF points have different symbols for the various plasma currents: black $\times$s for 1.2 MA, red diamonds for 1.0 MA, green asterisks for 0.8 MA and black triangles for 0.6 MA.

Fig. 3 Plasma parameter time histories for a 4.7 T (red dash-dot-dot-dot line) and a 4.5 T (green solid line) discharge.

Fig. 4 The toroidal rotation velocity (red dots) and the change in the plasma stored energy (green asterisks) as a function of toroidal magnetic field (resonance location) for a series of similar 0.8 MA discharges, between 0.75 and 0.95 s (top frame) and between 1.0 and 1.2 s (bottom frame).

Fig. 5 The time evolution of the electron density profile (top frame) and the x-ray brightness profile (bottom frame) during the ITB phase. The bottom axis label indicates the major radius while the top axis label shows the equivalent minor radius.

Fig. 6 Three views of the toroidal rotation velocity time histories for the 4.5 T discharge of Fig.3. The central view is shown by the solid black line, the view 10.4 cm above (10.3 cm below) the midplane is depicted by the red diamonds (green asterisks). Sight lines for the two off-axis views, superimposed on the magnetic flux surfaces, are shown in the upper right corner.

Fig. 7 The calculated neo-classical impurity toroidal rotation velocity profile (with E_r=0) before the ITB formation is shown by the red curve in the top frame, with the observed points shown as green dots. In the bottom frame are the same quantities during the ITB phase.

Fig. 8 Plasma parameter time histories for an Ohmic H-mode discharge with an ITB. In the top frame in red is the ratio of the central to edge electron density, and in green is the central soft x-ray emission. In the middle panel is the central ion temperature and in the bottom frame is the central toroidal rotation velocity.

Fig. 9 Electron density profiles for plasmas with ITBs; the dashed green line is for an Ohmic discharge, the solid red line is for an ICRF heated plasma with the resonance location at −9.9 cm and the purple dash-dot-dot-dot line is for a plasma with the ICRF resonance at −12.4 cm.

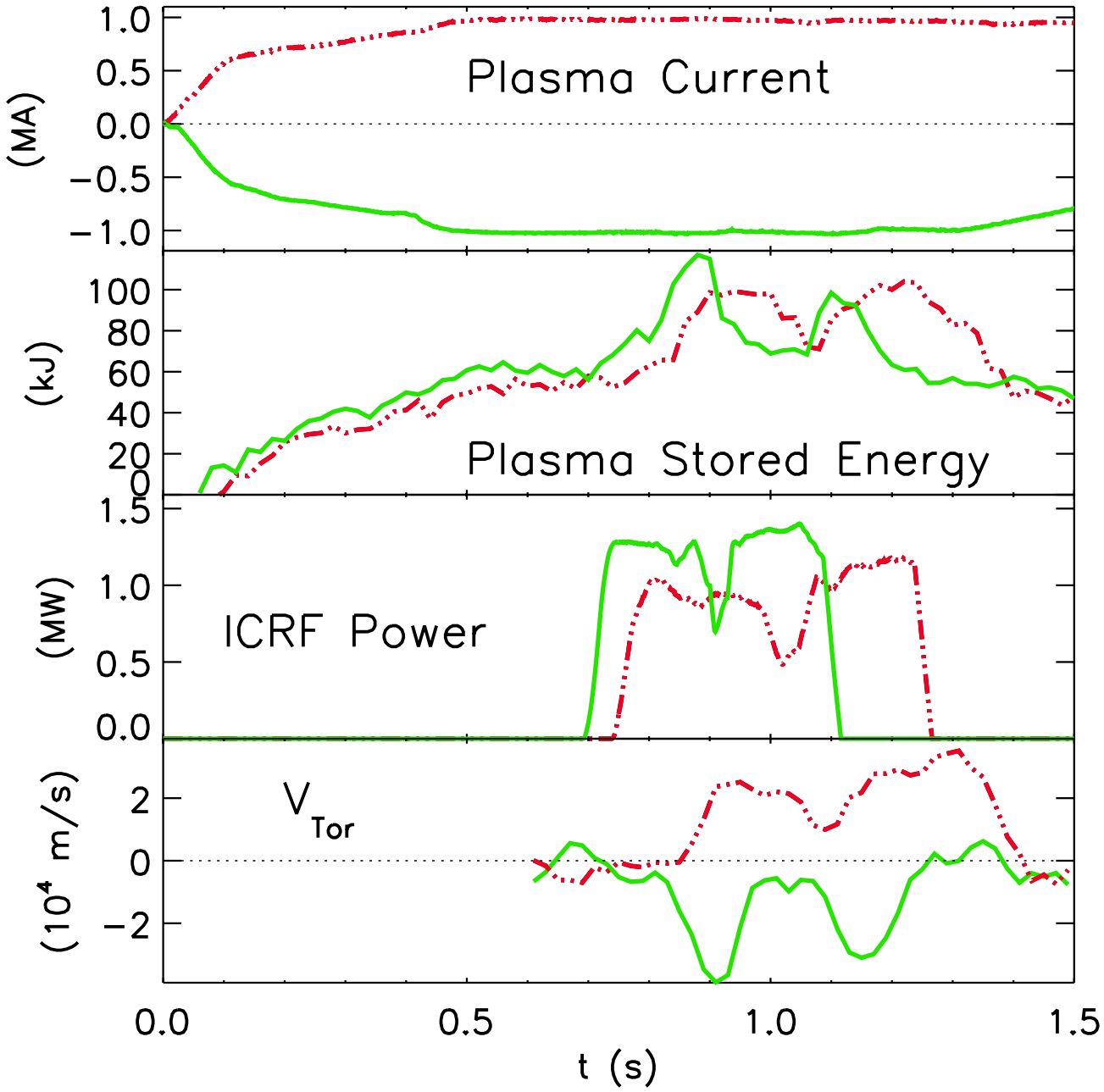
Plasma Current
(MA)
1.0
0.5
0.0
−0.5
−1.0
Plasma Stored Energy
(kJ)
100
80
60
40
20
0
ICRF Power
(MW)
1.5
1.0
0.5
0.0
V Tor
(10⁴ m/s)
2
0
−2
0.0
0.5
1.0
1.5
t (s)

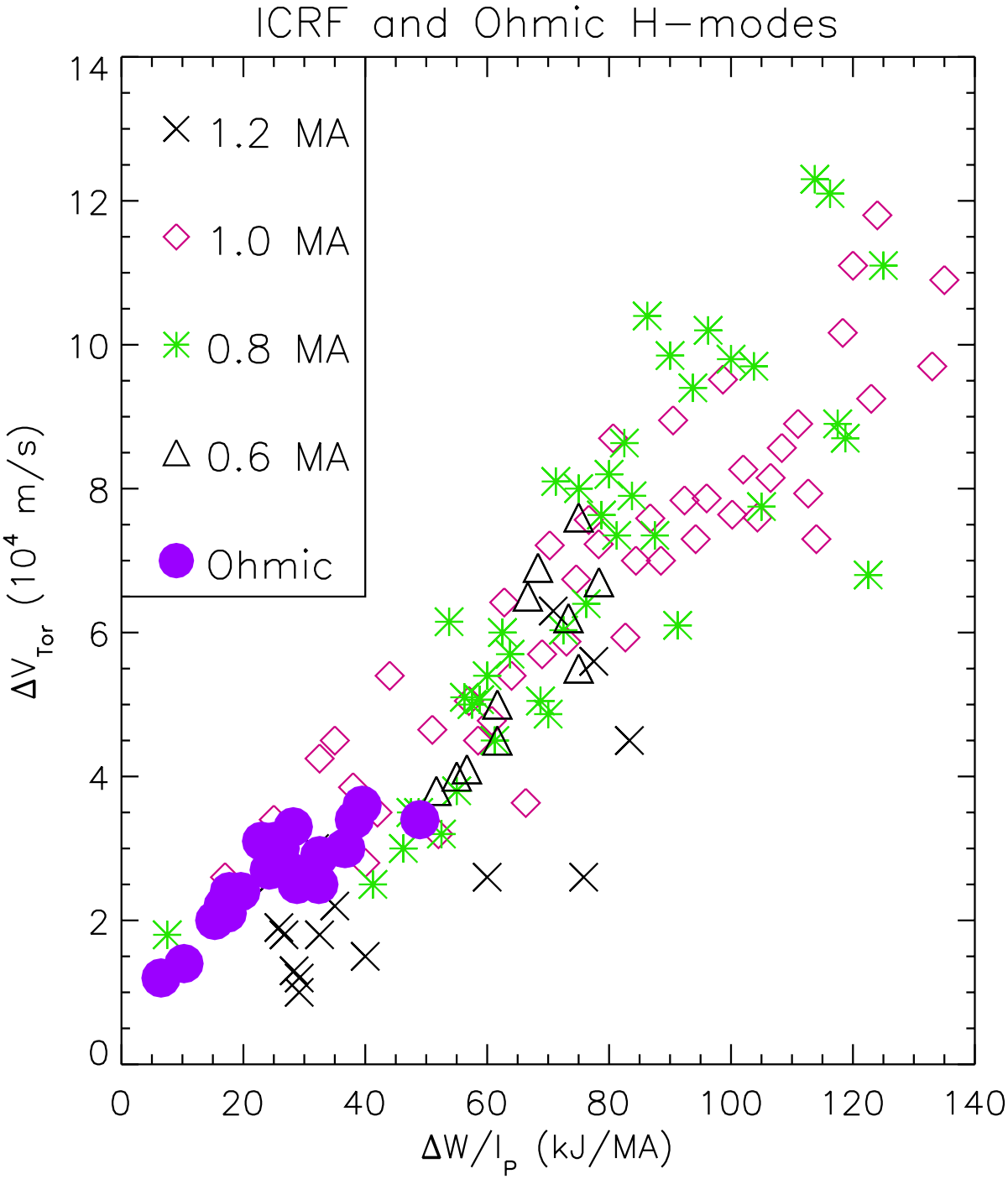
ICRF and Ohmic H−modes
1.2 MA
1.0 MA
0.8 MA
0.6 MA
Ohmic
ΔV_Tor (10^4 m/s)
ΔW/I_P (kJ/MA)
0
2
4
6
8
10
12
14
0
20
40
60
80
100
120
140

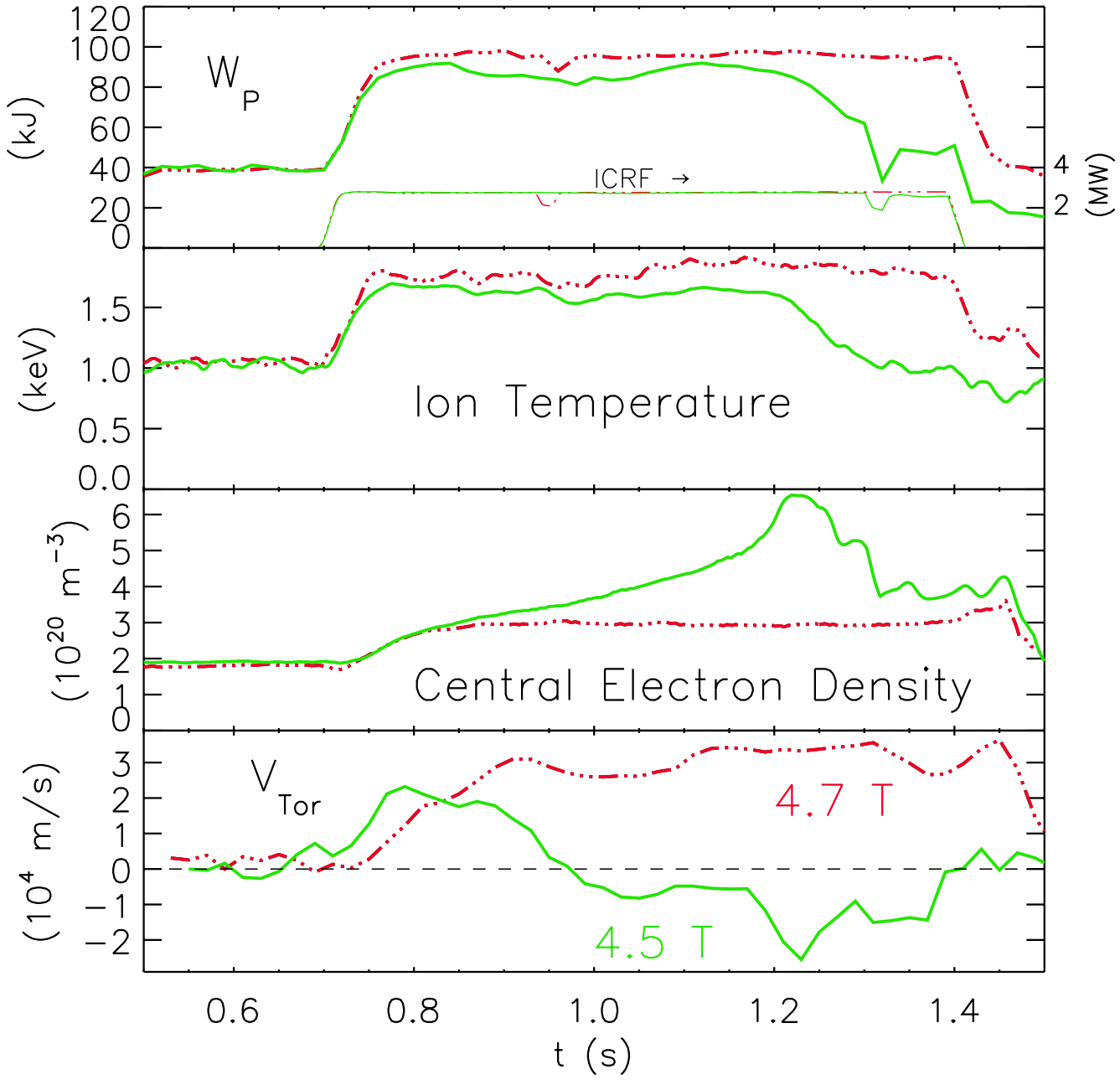
120
100
80
60
40
20
0
(kJ)
W_P
ICRF →
4
2
(MW)
1.5
1.0
0.5
0.0
(keV)
Ion Temperature
6
5
4
3
2
1
0
$(10^{20}\ m^{-3})$
Central Electron Density
3
2
1
0
−1
−2
$(10^4\ m/s)$
V_{Tor}
4.7 T
4.5 T
0.6
0.8
1.0
1.2
1.4
t (s)

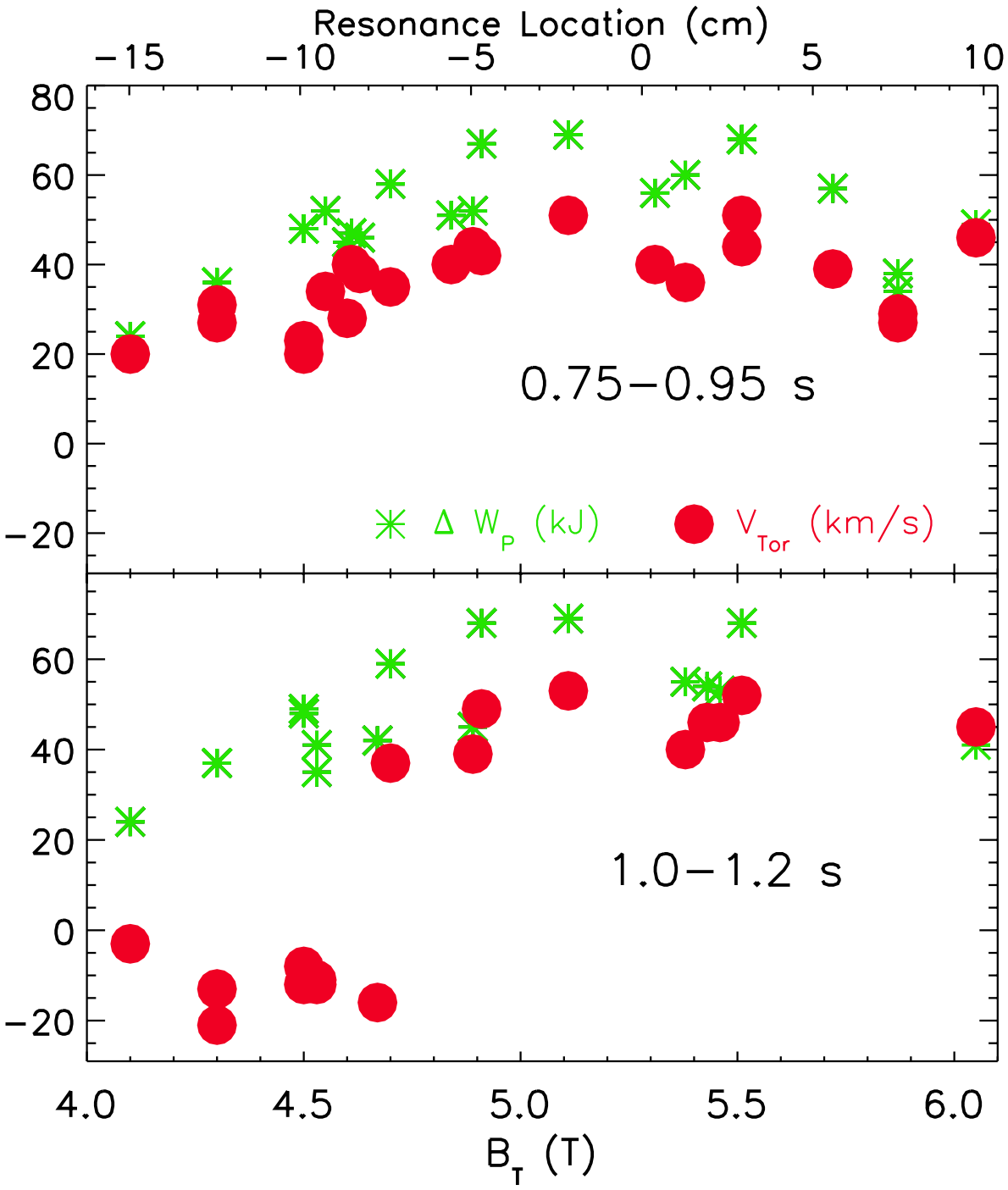
Resonance Location (cm)
−15
−10
−5
0
5
10
80
60
40
20
0
−20
0.75−0.95 s
Δ W_P (kJ)
V_Tor (km/s)
60
40
20
0
−20
1.0−1.2 s
4.0
4.5
5.0
5.5
6.0
B_T (T)

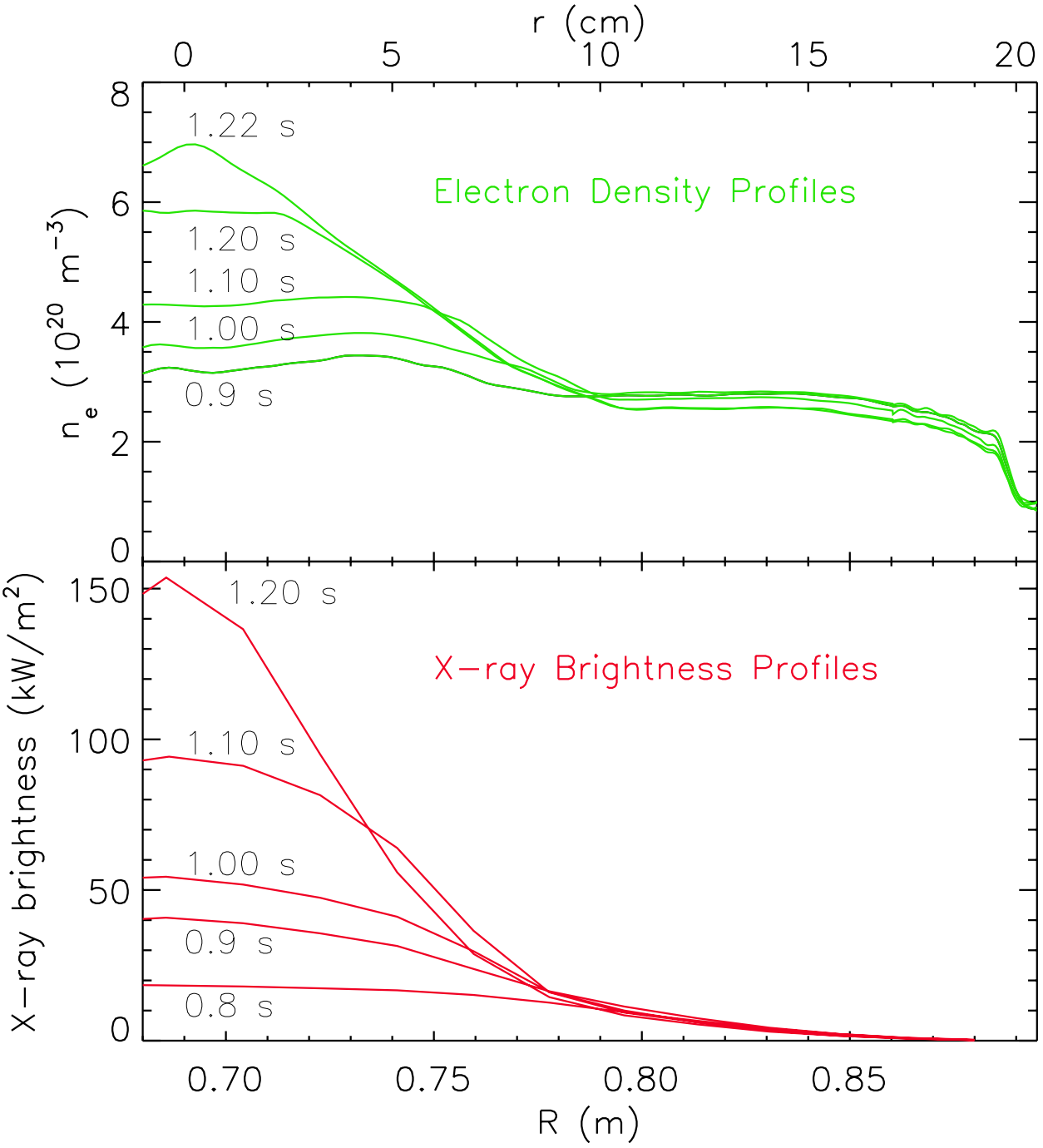
r (cm)
0
5
10
15
20
8
6
4
2
0
1.22 s
1.20 s
1.10 s
1.00 s
0.9 s
Electron Density Profiles
n_e (10^20 m^-3)
150
100
50
0
1.20 s
1.10 s
1.00 s
0.9 s
0.8 s
X-ray Brightness Profiles
X-ray brightness (kW/m^2)
0.70
0.75
0.80
0.85
R (m)

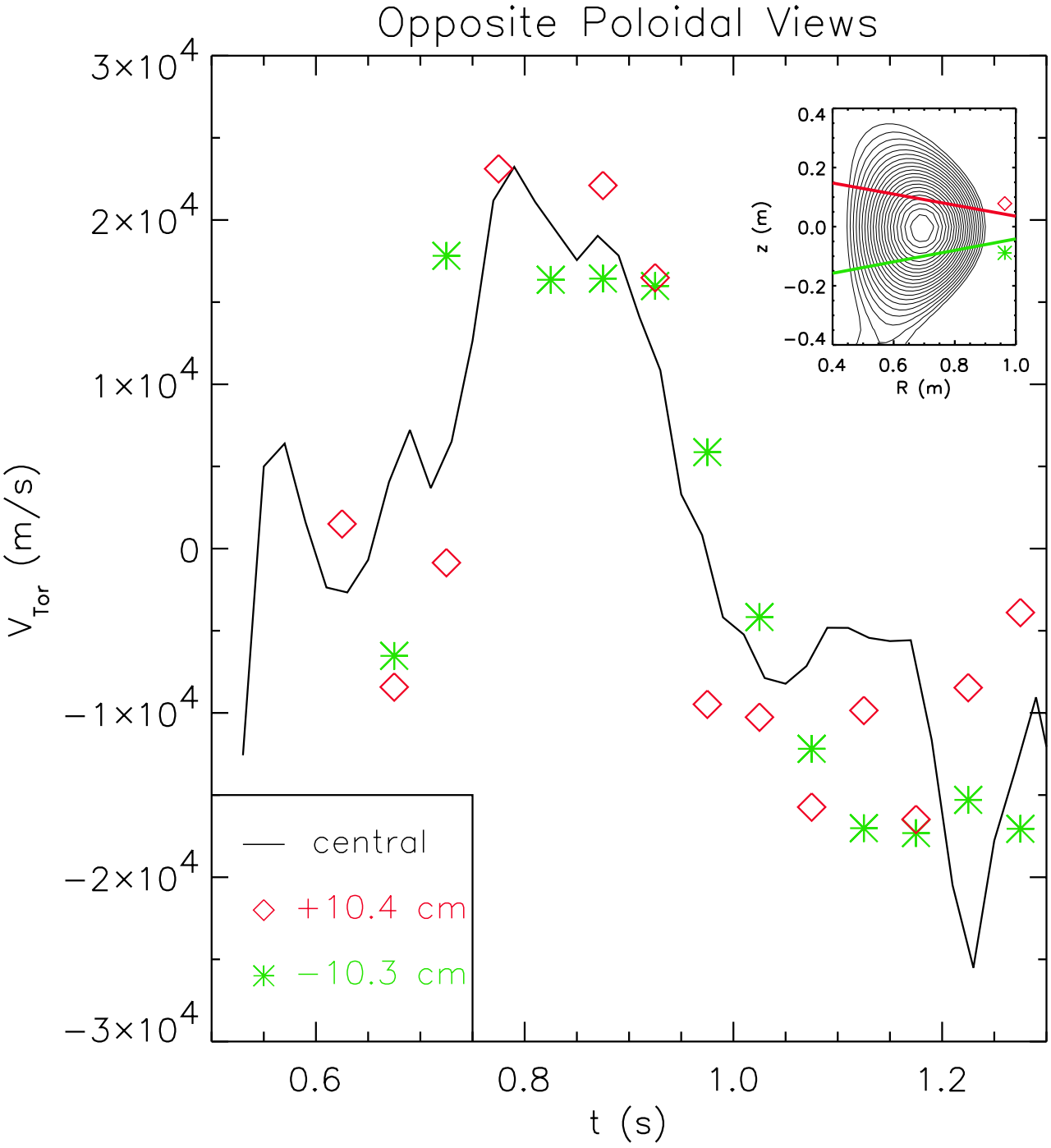
Opposite Poloidal Views
3×10^4
2×10^4
1×10^4
0
−1×10^4
−2×10^4
−3×10^4
V_Tor (m/s)
0.6
0.8
1.0
1.2
t (s)
central
+10.4 cm
−10.3 cm
0.4
0.2
0.0
−0.2
−0.4
z (m)
0.4
0.6
0.8
1.0
R (m)

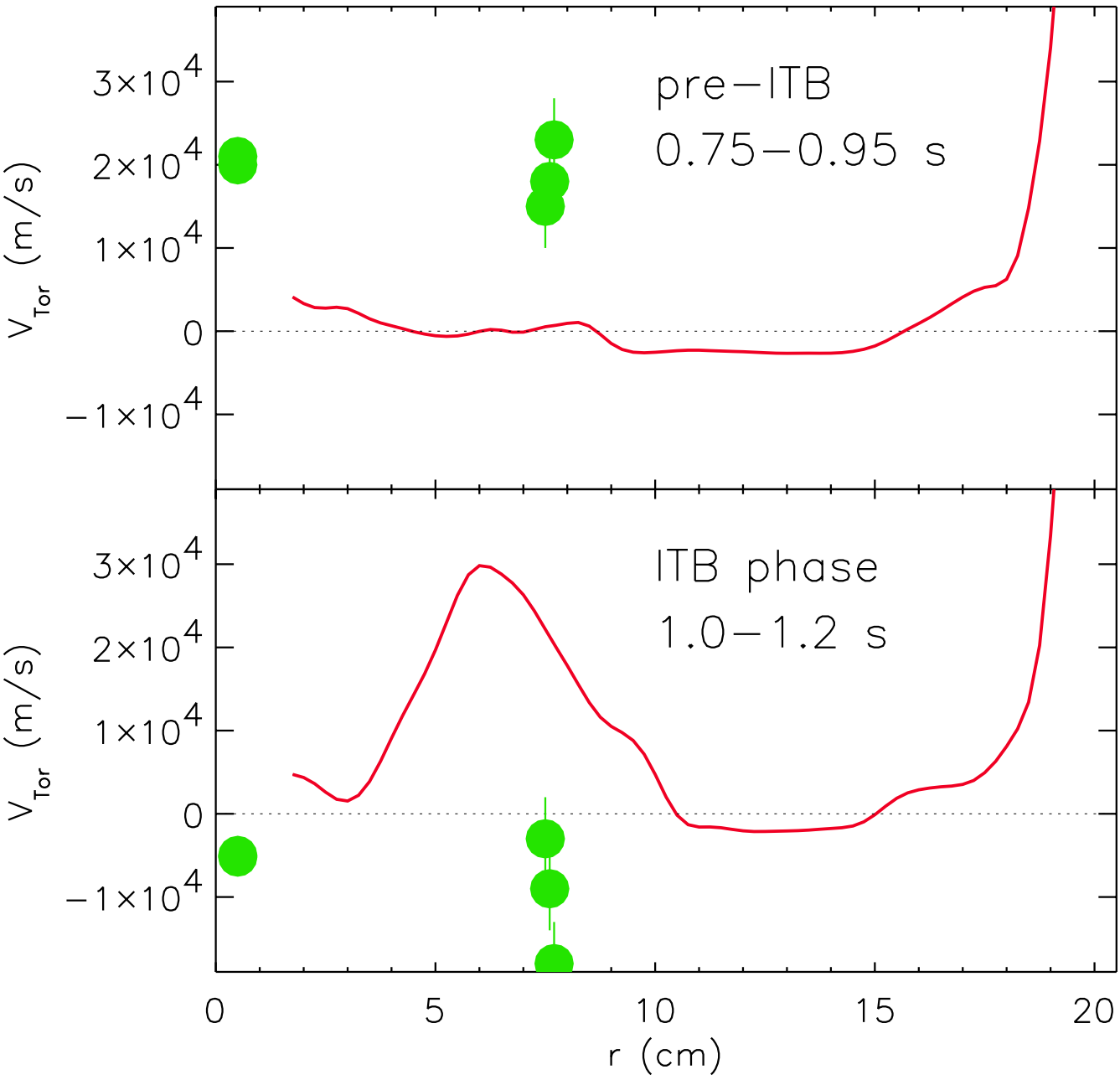
pre−ITB
0.75−0.95 s
ITB phase
1.0−1.2 s
V_Tor (m/s)
3×10^4
2×10^4
1×10^4
0
−1×10^4
0
5
10
15
20
r (cm)

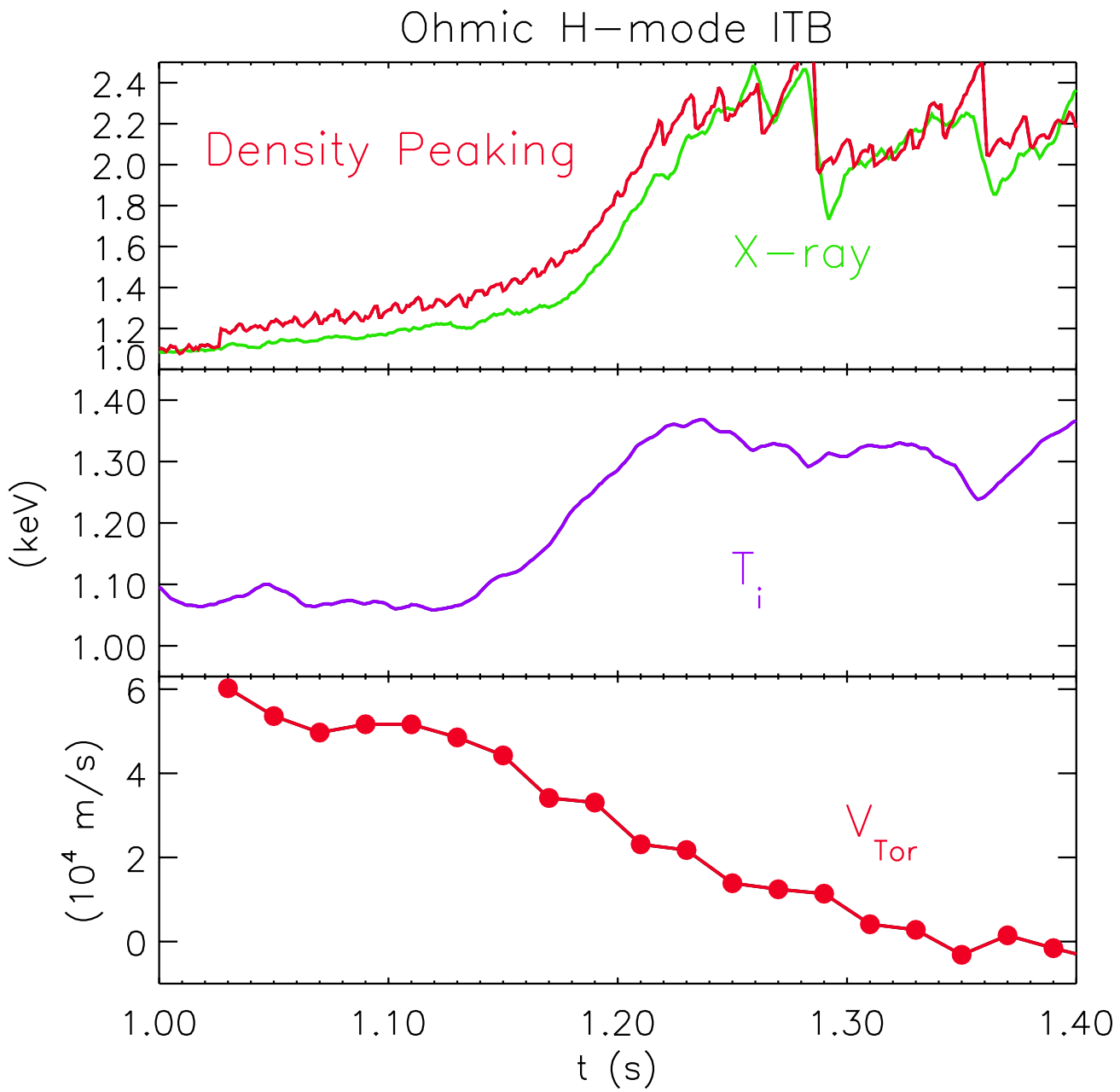
Ohmic H−mode ITB
Density Peaking
X−ray
T_i
V_{Tor}
(keV)
(10^4 m/s)
t (s)
2.4
2.2
2.0
1.8
1.6
1.4
1.2
1.0
1.40
1.30
1.20
1.10
1.00
6
4
2
0
1.00
1.10
1.20
1.30
1.40

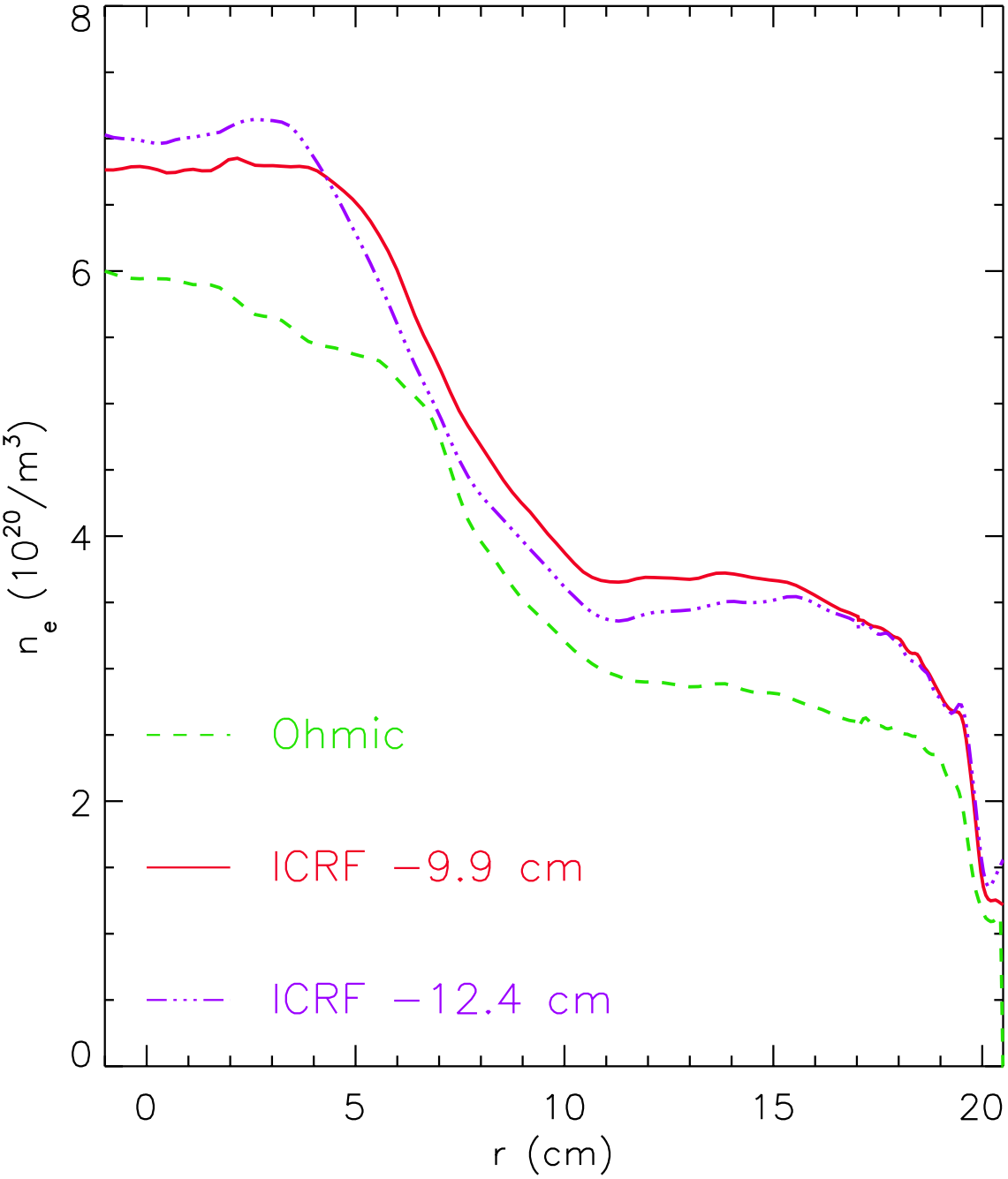
8
6
4
2
0
0
5
10
15
20
r (cm)
n_e (10^{20}/m^3)
Ohmic
ICRF −9.9 cm
ICRF −12.4 cm